Plasma Phys. Control. Fusion **51** (2009) 124034 (8pp) doi:10.1088/0741-3335/51/12/124034

Numerical simulation of hydrocarbon plasmas for nanoparticle formation and the growth of nanostructured thin films

Erik Neyts[1], **Maxie Eckert, Ming Mao and Annemie Bogaerts**

Research group PLASMANT, Department of Chemistry, University of Antwerp, Universiteitsplein 1, B-2610 Wilrijk, Belgium

E-mail: erik.neyts@ua.ac.be

Received 18 June 2009, in final form 14 September 2009
Published 11 November 2009
Online at stacks.iop.org/PPCF/51/124034

Abstract
This paper outlines two different numerical simulation approaches, carried out by our group, used for describing hydrocarbon plasmas in their applications for either nanoparticle formation in the plasma or the growth of nanostructured thin films, such as nanocrystalline diamond (NCD). A plasma model based on the fluid approach is utilized to study the initial mechanisms giving rise to nanoparticle formation in an acetylene plasma. The growth of NCD is investigated by molecular dynamics simulations, describing the interaction of the hydrocarbon species with a substrate.

1. Introduction

Hydrocarbon plasmas, such as in methane or acetylene, are widely used for the growth of different kinds of thin films, ranging from diamond and (ultra)nanocrystalline diamond ((U)NCD), over diamond-like carbon (DLC), to amorphous (hydrogenated) carbon (a-C : H) [1–4]. On the other hand, because of their large chemical reactivity, hydrocarbon plasmas can also give rise to the formation of nanoparticles in the plasma. The latter can be incorporated into the growing film, which is beneficial for some applications, but they can also cause damage [5]. Therefore, a fundamental understanding of the formation mechanisms of these nanoparticles is of uttermost importance to control their growth kinetics in the plasma. We try to obtain this better understanding by describing the detailed plasma chemistry giving rise to the nanoparticle formation by means of a fluid model. This fluid model, the basic processes and some important results will be outlined in the next section. Subsequently, it will be illustrated in section 3 how molecular dynamics (MD) simulations of plasma–surface interactions can give us more insight into the growth processes of carbon nanostructured thin films, such as (U)NCD.

[1] Author to whom any correspondence should be addressed.

0741-3335/09/124034+08$30.00 © 2009 IOP Publishing Ltd Printed in the UK

2. Fluid modeling for the description of nanoparticle formation in plasmas

2.1. Description of the fluid model

Fluid modeling is based on solving the continuity and transport equations (typically based on diffusion and migration) for the various plasma species (see equations (1) and (2), respectively):

$$\frac{\partial n_i}{\partial t} + \nabla \cdot \boldsymbol{J}_i = S_i, \tag{1}$$

$$\boldsymbol{J}_i = \pm \mu_i n_i \boldsymbol{E} - D_i \nabla n_i. \tag{2}$$

In these equations, n_i and J_i stand for the densities and fluxes of species i, S_i represents the net production rate determined by different production and loss terms. This includes all chemical reactions in the plasma, as well as the gas inlet and pumping. As mentioned above, the flux term is defined by the drift–diffusion approximation. D_i and μ_i are the species diffusion coefficients and mobilities, respectively, and E represents the instantaneous electric field. The (+) sign in the first term of equation (2) applies to the positive ions, whereas the (−) sign corresponds to the negative ions and electrons.

The electron energy is calculated by an energy conservation equation for the electron energy density, which is defined as $w_{\mathrm{e}} = n_{\mathrm{e}}\bar{\varepsilon}$ with $\bar{\varepsilon}$ the mean electron energy:

$$\frac{\partial w_{\mathrm{e}}}{\partial t} + \nabla \cdot \boldsymbol{J}_{w_{\mathrm{e}}} = -e\boldsymbol{J}_{\mathrm{e}} \cdot \boldsymbol{E} + S_{w_{\mathrm{e}}}. \tag{3}$$

$\boldsymbol{J}_{w_{\mathrm{e}}}$ is the electron energy density flux: $\boldsymbol{J}_{w_{\mathrm{e}}} = -\frac{5}{3}\mu_{\mathrm{e}} w_{\mathrm{e}} \boldsymbol{E} - \frac{5}{3} D_{\mathrm{e}} \nabla w_{\mathrm{e}}$.

Further, $S_{w_{\mathrm{e}}}$ is the source term of the electron energy density representing the loss and gain of electron energy due to collisions. The first term on the right-hand side of equation (3), which contains the electron charge $-e$, accounts for the Ohmic heating of the electrons due to the electric field. For the other, the so-called heavy particles, no energy conservation equation needs to be solved, because these species can be considered more or less in thermal equilibrium with the background gas, which is assumed to be at a certain temperature, typically slightly above room temperature.

These equations are solved together with the Poisson equation, in order to obtain a self-consistent electric field distribution:

$$\nabla \cdot (\boldsymbol{E}\varepsilon) = \rho, \tag{4}$$

where ε is the permittivity of the plasma and ρ is the space charge density obtained from the positive and negative ion densities and the electron density.

A fluid approach is particularly suitable for describing the detailed plasma chemistry, as in the case of investigating the initial mechanisms of nanoparticle formation in hydrocarbon plasmas. Indeed, a large number of different plasma species and chemical reactions can be included in the model, without too much computational effort. In the case of a C_2H_2 plasma, 78 different species (i.e. molecules, radicals, positive and negative ions, up to a maximum of 12 C atoms, as well as the electrons) were included in the model, as is presented in table 1. It should be noted that linear, branched and cyclic hydrocarbon species are included. The species included in the model were chosen based on extensive literature searches on the most important chemical reactions taking place in a C_2H_2 plasma, and the relevant species taking part in these reactions. In principle, the model can be extended to species containing more than 12 C atoms, but the chemistry will be very similar to that for the smaller species, and it would increase the calculation time. Overall, the general trends can be deduced from the species up to 12 C atoms.

Table 1. Overview of the different species included in the fluid model for a C_2H_2 plasma, besides electrons.

Molecules	Ions	Radicals
C_2H_2	$C_2H_2^+$, C_2H^+, CH^+, C_2^+, C^+	CH, CH_2, C_6H_3
C_4H_2, C_6H_2, C_8H_2, $C_{10}H_2$, $C_{12}H_2$, $C_6H_2^*$, $C_8H_2^*$, $C_{10}H_2^*$	C_4H^+, C_6H^+, C_8H^+, $C_4H_2^+$, $C_6H_2^+$, $C_8H_2^+$, $C_6H_4^+$, $C_8H_4^+$, $C_8H_6^+$, $C_{10}H_6^+$, $C_{12}H_6^+$	C_8H_6, $C_{10}H_6$, $C_{12}H_6$
H_2	H_2^+, H^+	H
C, C_2, H_2CC, C_2H_4, C_4H_4	$C_2H_3^+$, $C_2H_4^+$, $C_2H_5^+C_4H_3^+$, $C_4H_5^+$	C_2H_3, C_2H_5, C_4H_3
1-C_6H_4, 1-C_6H_6, A_1, A_2, PAHs		C_4H_5, n-C_6H_5, n-C_6H_7, A_{1-}, A_{2-}, A_1C_2 H
	C_2H^-, C_4H^-, C_6H^-, C_8H^-, $C_{10}H^-$, $C_{12}H^-$, H_2CC^-, $C_4H_2^-$, $C_6H_2^-$, $C_8H_2^-$, $C_8H_4^-$, $C_{10}H_4^-$	C_2H, C_4H, C_6H, C_8H, $C_{10}H$, $C_{12}H$

In total, 33 different electron-impact reactions, 305 different ion–neutral and 62 different neutral–neutral reactions are taken into account. The rate coefficients of the electron-impact reactions are obtained from the energy-dependent cross sections, in combination with the electron energy distribution function, as calculated by solving the Boltzmann equation in two-term approximation. The ion–neutral and neutral–neutral reactions are directly described by the rate coefficients. Note that not all data on reaction rate coefficients are available in the literature. Therefore, some assumptions had to be made. For instance, for the cluster growth through reaction of hydrocarbon anions ($C_{2n}H^-$, with $n = 1$–5) with C_2H_2, a constant value of 10^{-18} cm^3 s^{-1} was assumed for all the anions ($n = 1$–5). On the other hand, for the neutralization of these anions with cations, a scaling formula as a function of the electron affinity of the parent neutral radical of the anion and the ion–ion reduced mass was applied, as explained in [6]. For all species, diffusion coefficients and mobilities (for the charged species) had to be defined, as well as sticking probabilities at the walls. More details about the model (i.e. the transport coefficients and sticking coefficients at the walls, as well as a detailed list of all chemical reactions and their cross sections and rate coefficients) can be found in [7].

2.2. *Illustration of the results*

The model is applied here in one dimension, to a capacitively coupled RF discharge in a parallel plate reactor. The gap between the two electrodes is 2.5 cm and their diameter is assumed to be 13 cm. One electrode is connected to the power supply with a driving frequency of 13.56 MHz, whereas the other electrode is grounded. A pressure of 27 Pa and an electric power of 40 W are assumed. 8 sccm of pure C_2H_2 is fed into the reactor and a uniform gas temperature of 400 K is assumed. These conditions are chosen very similar to the experiment of Deschenaux *et al* [8] to allow a detailed comparison. Indeed, by comparing with experimental data, more specifically with mass spectra of the various positive and negative ions, some knowledge can be obtained on the relative importance of certain mechanisms initiating the nanoparticle formation, as illustrated below.

Figure 1 presents a comparison between our calculated species intensities (based on the fluxes toward the electrode) and mass spectral intensities for negative ions. The calculation results are obtained after the model reaches a steady state for these species. Of course, the nucleation process will still continue, and hence the concentrations of the larger species will still increase, but the species investigated in this study already reached steady state concentrations.

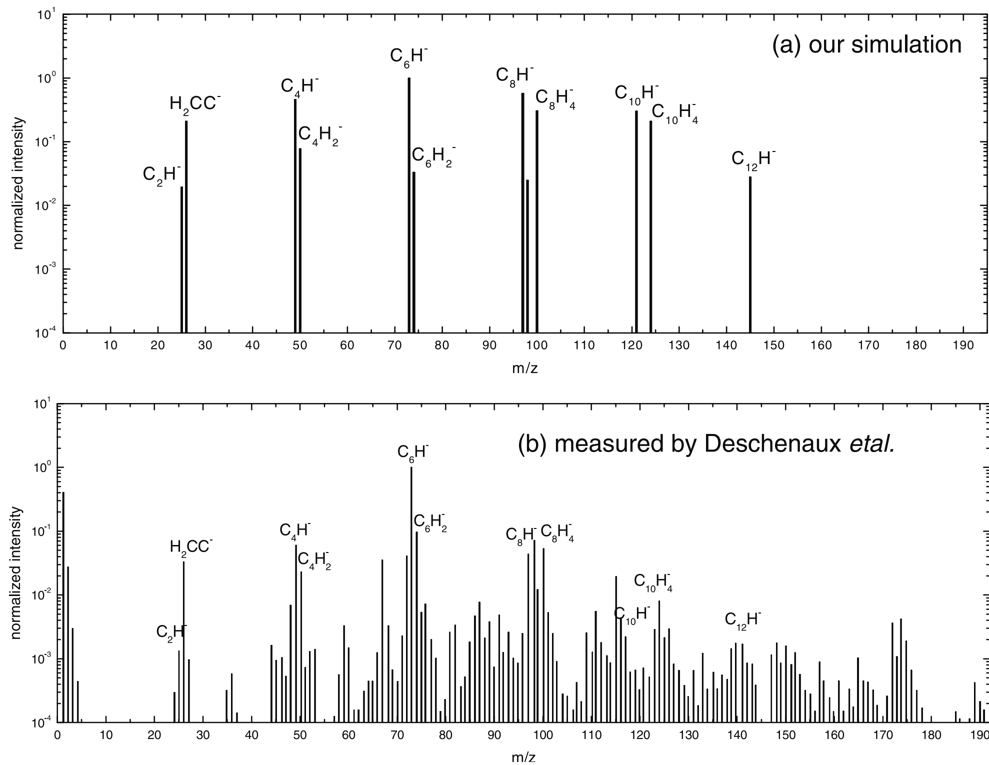

Figure 1. Calculated (*a*) and measured (*b*) mass spectra of the negative ions in a capacitively coupled radiofrequency discharge, operating in acetylene at 27 Pa, 13.56 MHz and 40 W (adapted from [6] with kind permission of IOP Publishing).

It is not clear from [8] whether steady state concentrations were also obtained in the experiment, but it was mentioned that no clear change in the measured electrode voltage was observed during the formation of powders.

The mass spectra, as measured by Deschenaux *et al*, contain significantly more peaks than the simulated spectra, illustrating that a lot of different species are present in the plasma. However, the most important peaks are also observed in the simulated spectra, and the relative intensities show very similar trends. Indeed, the C_6H^- ion is found to be the dominant negative ion, whereas in our previous model for a C_2H_2 plasma [6], the C_2H^- ion appeared to have the largest intensity and a decreasing trend toward larger negative ions was predicted [6]. This illustrates that some mechanisms were not yet included in our previous model, which turn out to be important in the plasma. These new mechanisms have been proposed in our recent paper [7]. Indeed, in our previous model only the so-called Winchester mechanism [5] was included for anion growth, i.e. the primary C_2H^- ions, generated through electron-impact dissociative attachment on C_2H_2, can trigger a consecutive chain of polymerization reactions with C_2H_2 insertion to form larger anions $C_{2n}H^-$ ($n = 2$–6). However, this yielded a decreasing trend toward larger anions [6]. Therefore, we proposed a new mechanism, based on dissociative electron attachment to larger hydrocarbon molecules ($C_{2n}H_2$; $n = 2$–5), and more specifically to branched $C_{2n}H_2$ molecules ($n > 2$). We suggest that these branched molecules are formed in the polymerization process of $C_{2n}H_2$ growth, where the C_2H radical is not only attached to the end C atoms (yielding linear structures) but also to the middle C

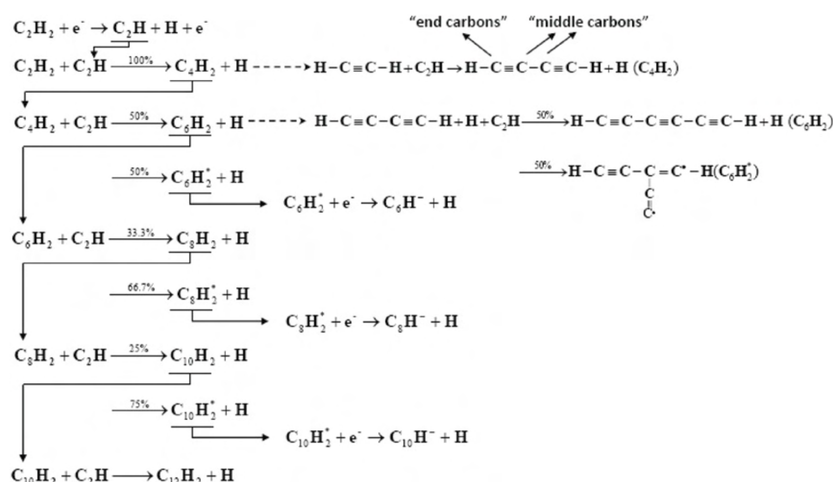

Figure 2. Schematic diagram of the proposed new mechanism for negative ion $C_{2n}H^-$ formation (adapted from [6] with kind permission of IOP Publishing).

atoms, thereby indeed giving rise to branched molecules. This mechanism is schematically illustrated in figure 2. Assuming that these branched molecules are characterized by a higher reactivity, giving enhanced dissociative electron attachment, this can explain why the C_6H^- ions have the highest intensity (see [8] for a more detailed discussion).

This example illustrates that the detailed plasma chemistry can be investigated in fluid modeling, and new mechanisms can be proposed by comparing with experimental data. Such investigations are important, as these reactions are considered as the initial mechanisms toward nanoparticle formation and growth in C_2H_2 plasmas.

3. MD simulations for the plasma-based growth of nanostructured thin films

3.1. Description of MD simulations

We simulate the formation of the carbon materials using classical MD, combined with Metropolis Monte Carlo (MMC). In a MD simulation, the time evolution of a set of interacting atoms is followed by calculating their equations of motion. Forces between the atoms are calculated as the negative of the gradient of a suitable interatomic potential energy function. The parameters used in the interatomic potential are fitted to *ab initio* and experimental data for a database of structures, usually including both solid state structures and gas phase molecules. The interatomic potentials used in these studies allow chemical bonds to be broken and formed as the simulation proceeds. The boundary conditions of the simulation determine the simulation ensemble. Although classical MD simulations are less accurate compared with *ab initio* simulations, they allow the simulation of thousands to even millions of atoms over relatively long timescales, which is not reachable by more accurate, i.e. *ab initio*, methodologies. This offers the possibility of simulating dynamic processes such as the nucleation and growth of materials on the atomic scale.

The equations of motion are integrated using the Velocity Verlet algorithm [9]. The time step used is set in the order of 0.1 fs.

Whereas the MD part of the code simulates impacts of growth species onto the surface on a timescale of picoseconds, the MMC algorithm simulates the slower relaxation processes.

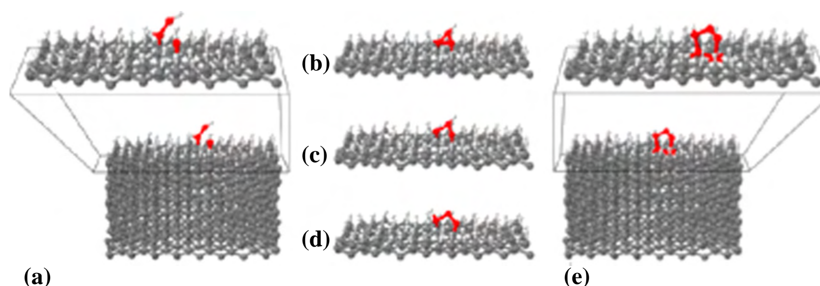

Figure 3. The formation of a diamond six ring as predicted by the MMC algorithm.

(This figure is in colour only in the electronic version)

Indeed, relaxation processes occur on the microsecond timescale, and hence cannot be simulated by MD alone. Typical MD calculation times are in the order of weeks or months to reach the nanosecond timescale.

For the growth of (U)NCD thin films, the substrate temperature is set to 1100 K, which is typical for a microwave plasma enhanced CVD (MWCVD) setup. The MMC algorithm operates on the adatoms in the system, i.e. all atoms which cannot be classified as 'crystalline' [10]. These adatoms, as well as their local environment, are allowed to move randomly in the MMC simulation. After the MMC simulation, a new particle impact is initiated using MD. The interatomic potential used is the Brenner potential for hydrocarbons [11].

3.2. Growth of (U)NCD

The combined MD–MMC simulations were performed for hydrocarbon species that are important for the microwave PECVD based growth of (U)NCD thin films at partially hydrogenated diamond surfaces. As an example, we consider here the combination of a C atom and a C_2H_2 molecule on a diamond (1 1 1) 1 × 1 surface [10].

The configuration as shown in figure 3(*a*) is obtained by consecutive MD impacts of a C atom and a C_2H_2 molecule on a partially hydrogenated diamond (1 1 1) 1 × 1 surface. These two species are known to be important growth species for (U)NCD films [10]. Before the impacts, this diamond surface contains three dangling bonds that are located close to each other. As shown in figure 3(*a*), both the C atom and the C_2H_2 molecule are bonded with a single bond to the diamond (1 1 1) 1 × 1 surface, which is the most probable configuration at substrate temperatures relevant for the deposition of (U)NCD, i.e. at substrate temperatures above 700 K. At the beginning of the MMC simulation, the simulation cell contains five adatoms (see figure 3): three carbon adatoms, highlighted in red, and two hydrogen atoms that are bonded to the carbon adatoms.. Also the two diamond surface atoms that are bonded to the adatoms and one cluster (originating from the C_2H_2 molecule) are allowed to move.

The MMC simulation moves the system from state to state. Figures 3(*b*)–(*d*) illustrate the selected snapshots of accepted configurations. The formation of a new carbon six ring which is characteristic of the diamond crystal structure, is shown in figures 3(*b*) and (*c*). First (figure 3(*b*)) an energetically unfavorable carbon three ring is formed. The carbon–carbon bond breaking (figure 3(*c*)) therefore leads to a decrease in the potential energy. After this three-ring formation, no further carbon–carbon bonds are broken or formed. Next, one of the hydrogen adatoms is displaced (see figure 3(*d*)), such that the two hydrogen adatoms are bonded to the same carbon adatom. Figure 3(*e*) shows the final MMC configuration. The

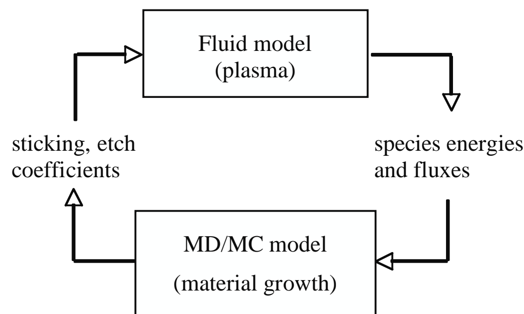

Figure 4. Schematic diagram of the future coupling between fluid and MD simulations.

formation of the diamond six ring pursues the diamond crystal structure: the three carbon adatoms are repositioned according to the diamond structure. The present example illustrates that these combined MD/MMC simulations are useful to unravel the (U)NCD thin film growth mechanisms on the atomic level.

The formation of the configurations resulting from the MMC simulations is verified by additional MD simulations. It is found that both the MD and MMC simulations lead to the same formation of carbon–carbon bonds, but the MD simulations need much longer time to reach the same result. The obtained boost factor, based on the time needed to reach similar configurations in the MD and MMC simulation, was estimated to be one order of magnitude [10].

4. Conclusion

This paper focuses on two different numerical simulation approaches for describing hydrocarbon plasmas to be used for the formation and growth of carbon nanoparticles or nanostructured materials. A fluid model is used to study the initial mechanisms leading to nanoparticle formation in acetylene capacitively coupled RF discharges. It is illustrated that the detailed plasma chemistry can be investigated with fluid modeling, and new mechanisms can be proposed by comparing with experimental data. MD simulations are used for describing plasma–surface interactions. The capabilities of this simulation method are illustrated for the growth of (U)NCD thin films.

In the near future, we plan to combine fluid and MD simulations. More specifically, the output of a fluid model, i.e. fluxes (and energies) of the various plasma species arriving at a substrate, can be used as input for MD simulations to describe thin film growth. Vice versa, MD simulations can provide data on sticking and reaction probabilities of the various plasma species at the walls, which can serve as boundary conditions for the fluid modeling. This is schematically illustrated in figure 4.

In the past, we have already illustrated such an approach for the growth of amorphous carbon films (although the fluxes of the bombarding species were then adopted from experiments instead of plasma simulations) [12]. In the near future, such a coupling between fluid and MD simulations is also planned for the growth of (U)NCD thin films. Because these films are typically grown in microwave plasmas, we are currently working on a fluid model for a microwave plasma, and the calculated fluxes and energies of the plasma species bombarding the substrate will serve as input for the MD simulations. Nevertheless, one has to keep in mind that the time between successive impacts, as deduced from the fluxes of bombarding species, is relatively long, and that this timescale will be too long for MD simulations. This

problem can be partly solved by coupling the MD method with the MMC approach, although the latter does not include time information. An alternative, and more realistic, approach is to use the relative fluxes of the impacting species as an input in the MD simulations. With this information it can be defined based on random numbers which species will successively bombard the surface and give rise to the growing film.

The back-coupling of MD simulations into the fluid model is more straightforward. Indeed, the MD simulations can first be carried out to provide a list of sticking coefficients of different species on specified substrates, and these data can then subsequently be used as an input in the fluid model. This is particularly interesting because sticking coefficients are not always available in the literature, and they have great impact on the calculated species densities. For (U)NCD thin films, we have already performed detailed studies on such sticking coefficients [13, 14], and they are currently being used as input data in our fluid simulations. In this way, we hope that a more complete and self-consistent picture of both the plasma and the plasma–surface interactions (for applications of plasma deposition as well as etching) can be obtained.

Acknowledgments

E Neyts acknowledges financial support from the Fund for Scientific Research Flanders (FWO). M Eckert is indebted to the Institute for the Promotion of Innovation by Science and Technology in Flanders (IWT-Flanders) for financial support. This work is also supported by an FWO project and an IAP-VI project of the Prime Minister's Office. Finally, the calculation support of the core facility CALCUA, provided by the University of Antwerp, is gratefully acknowledged.

References

[1] Hiramatsu M, Lau C H, Bennett A and Foord J S 2002 *Thin Solid Films* **407** 18
[2] Robertson J 2002 *Mater. Sci. Eng.* **R37** 129
[3] Malesevic A, Vitchev R, Schouteden K, Volodin A, Zhang L, Van Tendeloo G, Vanhulsel A and Van Haesendonck C 2008 *Nanotechnology* **19** 305604
[4] Cantoro M, Hofmann S, Pisana S, Scardaci V, Parvez A, Ducati C, Ferrari A C, Blackburn A M, Wang K-Y and Robertson J 2006 *Nano Lett.* **6** 1107
[5] Ostrikov K 2005 *Rev. Mod. Phys.* **77** 489
[6] De Bleecker K, Bogaerts A and Goedheer W 2006 *Phys. Rev.* E **73** 026405
[7] Mao M, Benedikt J, Consoli A and Bogaerts A 2008 *J. Phys. D: Appl. Phys.* **41** 225201
[8] Deschenaux Ch, Affolter A, Magni D, Hollenstein Ch and Fayet P 1999 *J. Phys. D: Appl. Phys.* **32** 1876
[9] Swope W C, Andersen H C, Berens P H and Wilson K R 1982 *J. Chem. Phys.* **76** 637
[10] Eckert M, Neyts E and Bogaerts A 2009 *Cryst. Eng. Commun.* **11** 1597
[11] Brenner D W 1990 *Phys. Rev.* B **42** 9458
[12] Neyts E, Bogaerts A and van de Sanden M C M 2006 *Appl. Phys. Lett.* **88** 141922
[13] Eckert M, Neyts E and Bogaerts A 2008 *J. Phys. D: Appl. Phys.* **41** 032006
[14] Eckert M, Neyts E and Bogaerts A 2008 *Chem. Vapor Depos.* **14** 213